


Growth of a highly ordered inhomogeneous kinetically trapped molecular monolayer

Sylvie Rangan,¹ Peter Kim,¹ Charles Ruggieri,¹ Stephen Whitelam,² and Robert A. Bartynski¹

¹*Department of Physics and Astronomy and Laboratory for Surface Modification, Rutgers University, 136 Frelinghuysen Road, Piscataway, New Jersey 08854, USA*

²*Molecular Foundry, Lawrence Berkeley National Laboratory, 1 Cyclotron Road, Berkeley, California 94720, USA*

 (Received 11 November 2018; revised manuscript received 1 October 2019; published 12 December 2019)

It is often assumed that the self-assembly of organic molecules on a noble-metal surface results in a structure that is in thermodynamic equilibrium. Here, using scanning tunnel microscopy, we observe instead a highly ordered *metastable* striped monolayer phase of zinc tetraphenylporphyrin, self-assembled at 300 K on Ag(100). The usually reported stable square phase is found only after higher-temperature annealing. We use a statistical mechanical model to reveal a possible molecular mechanism for this process, in which the competition of molecule and substrate interactions at the growth front leads to the growth of a kinetically trapped inhomogeneous ordered structure. Our proposed mechanism rests only on simple features of molecular geometry and interactions, and the resulting principles could be used to promote particular outcomes of growth in other examples of molecular assembly at surfaces.

DOI: [10.1103/PhysRevB.100.245411](https://doi.org/10.1103/PhysRevB.100.245411)

I. INTRODUCTION

The interface between organic molecules and metal or oxide surfaces is critical to a wide array of emerging fields, including organic or molecular electronics [1–3], gas sensing [4–7], catalysis [8–10], and photovoltaics [11–14]. Molecular self-assembly on single-crystal surfaces is a particularly interesting “bottom-up” pathway to the controlled growth of two-dimensional (2D) systems with a high degree of long-range order and many possible choices of molecular units and substrates [15,16]. Moreover, molecular self-assembly can serve as a precursor to the formation of highly ordered covalently bonded molecular units in order to build delocalized 2D systems, typically via surface-mediated chemistry [15–20]. While there have been many studies characterizing the self-assembly process of organic molecules at metal surfaces, the manner in which the competition between substrate-molecule interactions and intermolecular forces impacts molecular arrangement during overlayer growth remains poorly understood.

The self-assembly of organic molecules on noble-metal surfaces is often analyzed under the assumption that the molecular adsorbates have sufficient mobility to reach the configurations characteristic of thermodynamic equilibrium. Often, this is the case. For example, at room temperature a monolayer of metal-centered tetraphenylporphyrins (TPPs), a molecule with fourfold symmetry having high mobility on metal surfaces, will generally assemble into a thermodynamically stable, highly ordered, nearly square array, locked in place by T stacking of the phenyls on neighboring molecules [21–25]. In such studies, the surface is viewed primarily as a rigid support for self-assembly, having only a minor influence on the unit cell size and the registry of the molecular array.

In this work we examine the self-assembly of a ZnTPP monolayer on an Ag(100) surface at room temperature and demonstrate how kinetic factors can lead to an unusual, highly ordered inhomogeneous metastable molecular array

that relaxes to the thermodynamically favored configuration upon modest annealing. Monte Carlo simulations of a simple model of surface-mediated self-assembly reproduce this behavior and reveal the hierarchy of molecule-molecule and molecule-surface interactions required to promote particular outcomes of growth. The growth mechanism suggested by our simulations is relevant to other examples of growth on a structured surface and could, in principle, be modified to grow specific kinetically controlled patterns.

II. EXPERIMENTAL DETAILS

Scanning tunneling microscopy (STM) measurements were performed in a UHV environment at pressures better than 5×10^{-10} Torr with an Omicron variable temperature STM unit. The STM chamber was equipped with an argon ion sputtering source and a heater mounted to the manipulator arm in contact with the sample, permitting preparation of the surface *in situ*. A clean and atomically flat Ag(100) single-crystal surface was achieved by performing cycles of argon ion sputtering ($3 \mu\text{A}$, 1500 V for 30 min) and annealing (500 °C for 30 min). The STM tip was electrochemically etched from tungsten wire (0.25 mm diameter). The images presented here were obtained in constant-current mode with the sample at room temperature. ZnTPP molecules [Frontier Scientific Zn(II) meso-Tetraphenylporphine > 95% purity] were deposited via sublimation in the same UHV environment using a Knudsen cell between 250 °C and 280 °C that was thoroughly degassed prior to deposition. We estimated the molecular deposition flux as 10^{11} molecules $\text{cm}^{-2} \text{s}^{-1}$, using coverage and deposition times from STM images. Images were processed using the WSXM 5.0 DEVELOP 6.4 software [26].

For the STM measurements, due to a combination of noise and drift during imaging, the uncertainties are conservatively

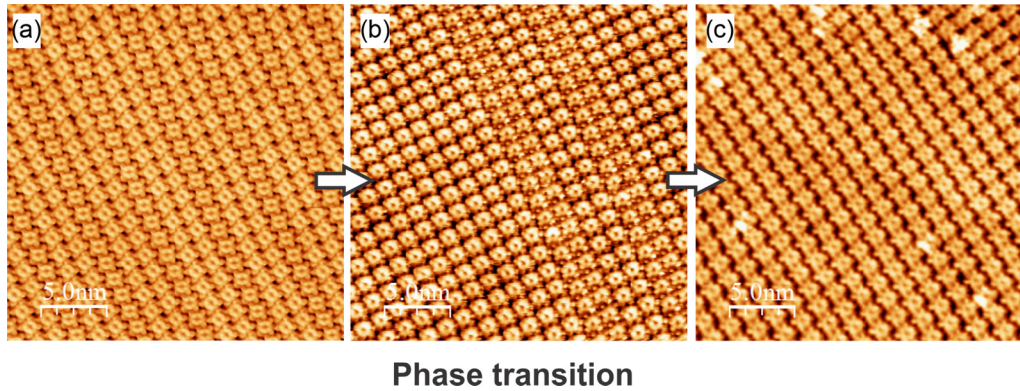


FIG. 1. Transformation of an ordered grown structure to a stable phase. (a) At room temperature, ZnTPP molecules assemble into a highly ordered kinetically trapped $[2 + 1]$ monolayer. (b) and (c) show that this structure transforms into a thermodynamically stable square phase upon annealing to 500 K. Dimensions: $25 \times 25 \text{ nm}^2$.

estimated as $\pm 0.1 \text{ \AA}$ for heights, $\pm 1 \text{ \AA}$ for lateral distances, and $\sim 3^\circ$ for angles.

The STM chamber is also equipped with a low-energy electron diffraction (LEED) system, with which the substrate surface high-symmetry directions are determined. These high-symmetry directions are subsequently used to orient molecular features of the STM images to the substrate atomic rows.

III. GROWTH OF INHOMOGENEOUS ORDERED STRUCTURES

STM images of a monolayer of ZnTPP on Ag(100) are shown in Figs. 1(a)–1(c). Upon successive anneals to 500 K, the as-deposited phase [Fig. 1(a)] progresses to an intermediate phase [Fig. 1(b)] and finally reaches a thermodynamically stable phase [Fig. 1(c)]. The molecular arrangement of Fig. 1(a) consists of two adjacent rows whose molecules form a square array and have the same azimuthal orientation and an adjacent third row where the molecules are displaced and rigidly rotated with respect to those of the other two rows. This three-row pattern repeats in the direction perpendicular to the rows and will be referred to as the $[2 + 1]$ configuration. Upon annealing, rows of the “+1” type transform into the square type, and eventually, the entire overlayer assumes the thermodynamically favored square phase.

The $[2 + 1]$ phase is unlike the typical ordered square arrays found for ZnTPP on other surfaces [21,22,24,25]. The square phase has been observed before for ZnTPP monolayers on Ag(100) using a “top-down” approach [24] in which a ZnTPP multilayer is annealed at 500 K to desorb the weakly bound molecular layers. This process leaves only a ZnTPP monolayer in contact with the substrate. An STM image of the square phase, along with geometric details and the registry of the overlayer with the crystallographic directions of the Ag(100) surface, are presented in Fig. 2(a). The corresponding information for the $[2 + 1]$ phase is presented in Fig. 2(b). Representative molecular diagrams, as well as the crystallographic directions of the underlying Ag(100) surface, are overlaid on the model. In both phases, as shown in Fig. 2(c), the molecules exhibit twofold rather than fourfold symmetry as a function of bias because alternating pyrrole groups of the

porphyrin macrocycle are tilted towards and away from the metal surface [27,28]. Following the schematic diagram of the molecule in Fig. 2(c), the open and solid circles represent the downward and upward tilted pyrroles, respectively, while the crosses indicate the location of the phenyl groups. Finally, the measured dimensions for each molecular adsorption model are given in Fig. 2(d).

For the $[2 + 1]$ phase, it is important to note that the part of the unit cell associated with the double-row portion of this phase, highlighted as a blue square, is identical to the unit cell of the square phase. The remaining part of the unit cell, denoted by red lines, has a length that is twice that of the blue unit cell. Therefore, the area of the $[2 + 1]$ unit cell is three times that of the square phase but possesses a basis of three molecules as opposed to one. Consequently, both the $[2 + 1]$ and square phases possess the same molecular coverage of $1/(20d^2) \approx 6 \times 10^{13} \text{ molecules/cm}^2$, where $d \approx 2.89 \text{ \AA}$ is the nearest-neighbor distance of the Ag(100) surface. Phase transitions of TPP assemblies were observed previously on metal surfaces but are accompanied by an alteration of the molecular coverage [29] or coadsorption of smaller species such as NO [30]. Here, the overlayer coverage remains fixed as the molecules rearrange to transform from the metastable phase to the thermodynamically preferred one.

Insights into why the $[2 + 1]$ phase assembles can be drawn from the STM images in Fig. 3. Figure 3(a) shows the typical long-range order observed on individual terraces. Each terrace is covered by a single domain of the $[2 + 1]$ phase, with the rows extending parallel to a straight step edge. Molecular orientation and periodicity along the rows are preserved for hundreds of nanometers; in the perpendicular direction, only a few errors of row stacking are observed. An example of a stacking fault can be seen in Fig. 3(b). This area is a zoomed-in view of the region delimited by the white rectangle in Fig. 3(a). The stacking error extends along the entire length of the row. Important information regarding the overlayer growth mode is provided by the STM image of a ZnTPP island on Ag(100), as seen in Fig. 3(c). That the molecules form islands is a clear indication of a net attractive interaction between the molecules. Moreover, this island nucleates at a substrate step edge and grows outward

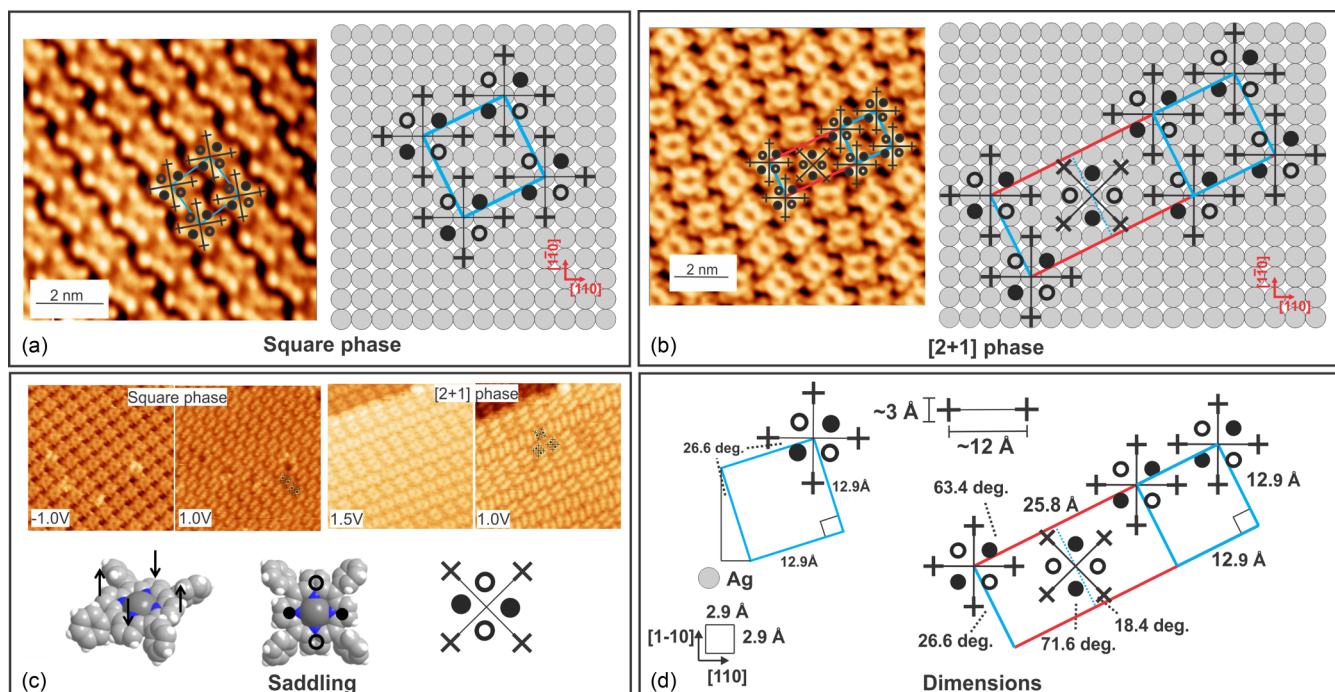


FIG. 2. STM images and proposed adsorption geometries for ZnTPP on Ag(100): (a) Square phase and (b) $[2 + 1]$ phase. (c) Characteristic ZnTPP twofold symmetry due to saddling as a function of bias: The positions of phenyls and pyrrole groups are represented by small crosses and circles, respectively. Open and solid circles represent downward and upward bending of the pyrrole groups, respectively. (d) Measured dimensions.

onto the terrace and along the step itself. As the growth front progresses along the terrace, the molecular rows adopt the strict $[2 + 1]$ pattern, indicating that as a molecule attaches to the growth front, its orientation and binding site are highly dependent on the nature of the previous molecular row: in the direction parallel to the step edge molecules keep the same adsorption mode, whereas in the direction perpendicular to the step edge, a $[2 + 1]$ alternation is favored.

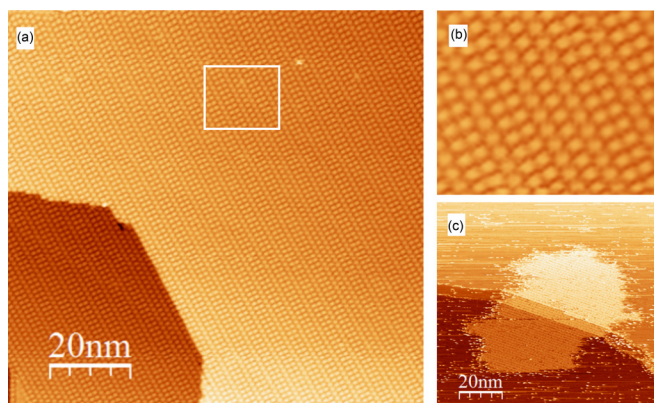


FIG. 3. Growth of an ordered metastable phase. (a) The $[2 + 1]$ phase is characterized by a long-range order on each terrace. (b) An enlargement of the area delimited by the white box in (a): the few visible stacking errors are propagated along entire columns. (c) Typical growth front for the molecular layer starting at step edges and propagating across the crystal terraces.

IV. A PROPOSED MECHANISM FOR GROWTH

The experiments described above show the growth of the inhomogeneous $[2 + 1]$ structure under conditions for which the homogeneous square phase is thermodynamically stable. In the remainder of this paper we describe a physical mechanism that could give rise to such behavior. We start by noting that intermolecular forces (T stacking of the mesophenyls of neighboring molecules) favor the homogeneous square phase [31]. We then hypothesize that, under the condition that molecular seeding at step edges is constraining growth, molecule-surface forces favor a striped phase. This hypothesis seems plausible given that there exists a mismatch between the lattice constants of the square phase and the metal substrate, a feature that favors modulation of a molecular pattern. We then show that this hypothesis implies an emergent mechanism that allows the formation of a *nonequilibrium* striped structure, under conditions such that the *equilibrium* structure is homogeneous. We therefore demonstrate the existence of a robust mechanism for the formation of modulated nonequilibrium patterns, given certain requirements on the intermolecular and molecule-surface forces. Additional molecular modeling is required to confirm the energetic hypothesis that underpins this model, but the significance of the following calculations is that they identify a particular (and nontrivial) nonequilibrium behavior given a set of energetic parameters.

Our proposed mechanism rests on the fact that, at the overlayer growth front, molecules possess fewer bonds than they do in the interior of the overlayer. The low-energy environment of a *growing* structure is therefore more likely to be dominated by molecule-surface interactions (which here we

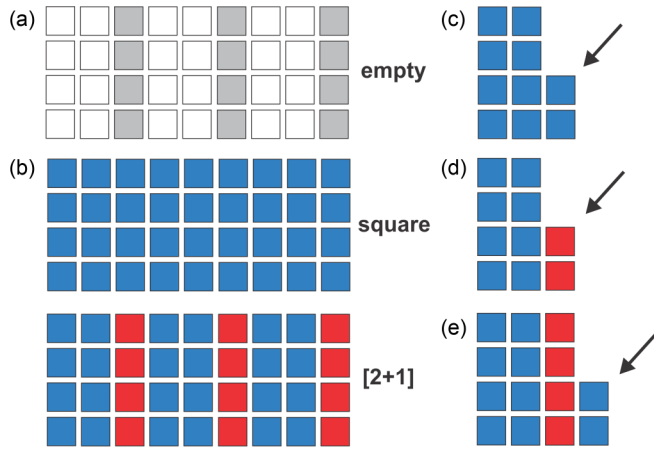


FIG. 4. Schematic model for ZnTPP self-assembly on Ag(100). (a) Effective modulation of the model Ag(100) surface. (b) Examples of the square and [2 + 1] structures; blue squares represent the molecular orientation characteristic of the square phase, while red squares represent molecular orientations observed in the “+1” part of the [2 + 1] phase. (c)–(e) Possible growth modes.

assume to favor the striped structure). Once the overlayer has grown, molecules in its interior possess more neighbors than they did at the growth front, so the low-energy environment felt by molecules in the *grown* structure is more likely to be dominated by intermolecular forces (which favor the square phase). Upon heating, molecules can, in principle, rearrange and lower their energy by adopting this arrangement.

Explicit calculation shows that this mechanism emerges from a particular hierarchy of molecular and substrate interactions. Consider Fig. 4, which shows a statistical mechanical model adapted from Ref. [32]. The model describes a square lattice (the substrate) whose sites can be vacant (white or gray) or occupied by a blue particle or a red particle. Blue and red particles stand for molecules of the same type in distinct orientations. Nearest-neighbor colored particles receive an energetic reward of $-\epsilon_s < 0$ or $-\epsilon_d < 0$ if they are the same color or different colors, respectively; we choose $\epsilon_s > \epsilon_d$ in order to favor homogenous structures. Vacant lattice sites receive an energetic reward $-\mu < 0$ relative to being occupied by a colored particle; μ functions as a chemical potential that influences the on-substrate coverage of particles. In addition, substrate sites possess an energetic bias for one of the particle types with the modulation shown in Fig. 4. On gray sites, red (blue) molecules receive an energy reward (penalty) $-\Delta_r < 0$ ($\Delta_b > 0$). On white sites, blue (red) molecules receive an energy reward (penalty) of $-\tilde{\Delta}_b < 0$ ($\tilde{\Delta}_r > 0$).

This model represents, in as simple a manner as possible, a set of molecules whose intermolecular interactions favor consistent orientations but whose interaction with a structured substrate favors alternating orientations with a particular modulation. Given such interactions, the following simple arguments indicate that it is possible to grow a metastable striped structure, whose modulation is controlled by interactions with the substrate, under conditions for which the homogenous phase is stable.

Equilibrium phases can be retrieved from the free energy per particle of a phase relative to that of the clean substrate.

For example, in the interior of the homogeneous (square, or \square) phase this energy is

$$E_{\square} = \mu - 2\epsilon_s + \frac{1}{3}(\Delta_b - 2\tilde{\Delta}_b), \quad (1)$$

and the free energy per particle in the interior of the striped ([2 + 1]) phase relative to that of the clean substrate is

$$E_{[2+1]} = \mu - \frac{2}{3}(\epsilon_d + 2\epsilon_s) - \frac{1}{3}(2\tilde{\Delta}_b + \Delta_r). \quad (2)$$

We shall consider conditions such that the homogeneous phase is stable with respect to the striped phase, i.e.,

$$E_{[2+1]} - E_{\square} = -\frac{2}{3}(\epsilon_d - \epsilon_s) - \frac{1}{3}(\Delta_r + \Delta_b) > 0. \quad (3)$$

Although the homogeneous phase is stable, it is possible to arrange for the *growth* of the homogenous phase to be less favorable energetically than the growth of the striped phase.

Consider the growth schematics shown in Fig. 4(c). The microscopic energy change upon extending the homogenous structure by the blue particle indicated by the arrow is

$$\delta E_{\square}^{\text{blue}} = \mu - 2\epsilon_s + \Delta_b. \quad (4)$$

On the other hand, the microscopic energy cost required to extend the striped phase shown in Fig. 4(d) by the indicated red particle is

$$\delta E_{[2+1]}^{\text{red}} = -\epsilon_s - \epsilon_d - \Delta_r + \mu, \quad (5)$$

and the cost incurred on placing the blue particle indicated in Fig. 4(e) is

$$\delta E_{[2+1]}^{\text{blue}} = -\epsilon_s - \epsilon_d - \tilde{\Delta}_b + \mu. \quad (6)$$

Thus, if $\delta E_{[2+1]}^{\text{red}} - \delta E_{\square}^{\text{blue}} < 0$, then extension of the [2 + 1] phase is favored with respect to extension of the homogenous phase, and we would expect to observe growth of the *metastable* striped phase rather than the *stable* homogenous phase.

V. SIMULATIONS CONFIRM THE PLAUSIBILITY OF THE PROPOSED GROWTH MECHANISM

Computer simulations bear out this expectation. We simulated the model using a dynamic Monte Carlo algorithm similar to that used in Ref. [32], adapted to include on-substrate molecular diffusion and rotation processes (see the Appendix). The surface was seeded with a row of molecules, representing the experimental observation that molecular islands nucleate at step edges [Fig. 3(c)], to allow us to study growth without waiting for step nucleation to occur. During the simulation, molecules are allowed to adsorb or desorb from the surface, and adsorbed molecules are allowed to diffuse and rotate. Growth is stopped when a chosen surface coverage is achieved. After growth, thermodynamic equilibrium is found using an annealing protocol.

Guided by the energetic arguments given in the previous section, we can identify parameter values for which we can grow a striped metastable overlayer that can be transformed into a homogeneous one upon annealing. An example of this behavior is shown in Fig. 5 for the set of parameters (measured in eV) $\epsilon_s = 3$, $\epsilon_d = 1$, $\Delta_r = 2$, $\Delta_b = 1$, $\tilde{\Delta}_r = 1$, $\tilde{\Delta}_b = 2$, and $\mu = 3$. These parameters are broadly compatible with energetics inferred from experimental measurements [29,33,34], but a precise mapping between model parameters

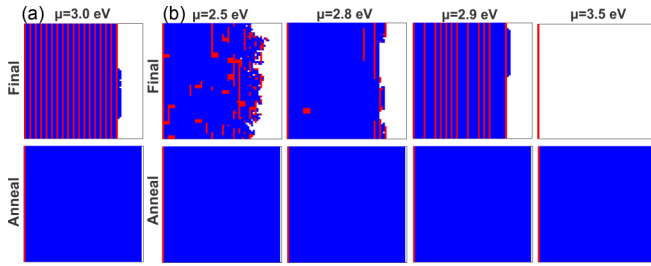


FIG. 5. (a) Monte Carlo simulations demonstrate the growth of a metastable striped phase (“final” denotes the outcome of growth) and its subsequent relaxation to a stable homogeneous phase under an annealing protocol (“anneal”). (b) For increasing values of the chemical potential μ we observe a steadily increasing barrier to nucleation of clusters on the surface. Parameters (in eV): $\epsilon_s = 3$, $\epsilon_d = 1$, $\Delta_r = 2$, $\Delta_b = 1$, $\tilde{\Delta}_r = 1$, and $\tilde{\Delta}_b = 2$. Rates: $R_{\text{ex}} = 10^{-5}$, $R_{\text{diff}} = 1$, and $R_{\text{rot}} = 1$.

and molecular energies is beyond the scope of this paper. We set the relative rates of exchange, diffusion, and rotation to $R_{\text{ex}} = 10^{-5}$, $R_{\text{diff}} = 1$, and $R_{\text{rot}} = 1$, respectively, enforcing the experimentally appropriate constraint that on-substrate diffusion and rotation happen much faster than the addition or removal of molecules from the surface. In this set of simulations we have $E_{[2+1]} - E_{\square} > 0$, so that the square phase is thermodynamically stable with respect to the striped phase, but $\delta E_{[2+1]}^{\text{red}} - \delta E_{\square}^{\text{blue}} < 0$, so we expect the metastable striped phase to grow faster than the stable homogeneous phase.

In agreement with this expectation, we observe upon simulation the growth of a metastable striped structure [Fig. 5(a)]. Growth under these conditions happens in a row-by-row manner, and we see the occasional presence of missing red rows (Fig. 8), similar to features seen in experiment [see Fig. 3(b)]. Upon completion of growth, we accelerate relaxation to equilibrium by allowing red and blue sites to interconvert using an algorithm that obeys detailed balance with respect to the same energy function as the growth algorithm. The result is that the striped phase transforms rapidly into the thermodynamically stable homogeneous blue phase, demonstrating the viability of our proposed mechanism.

The parameter μ controls the rate of nucleation and growth of the overlayer (Fig. 5). Whereas the growth front of Fig. 5(a) propagates preferentially in a row-by-row mode, for small μ the growth front exhibits large fluctuations, and we often observe the formation of a structure that is mostly blue. This is so because red rows are unstable to the replacement of a single red particle with a blue one: the energy cost to replace one red particle from a red row by a blue one is $\Delta_r + \Delta_b = 3$, which is unfavorable, but the energy needed to replace a red particle adjacent to the new blue particle is $2(\epsilon_d - \epsilon_s) + \Delta_r + \Delta_b = -1$, which is favorable. Thus, once a single red particle is converted to blue, the entire red row is destabilized and will readily transform to blue. For $\mu = 3.5$ eV, the energetic cost of molecular adsorption is increased so much that nucleation does not occur within our calculation time.

VI. CONCLUSION

In summary, we have observed the growth of a kinetically trapped but nonetheless highly ordered [2 + 1]

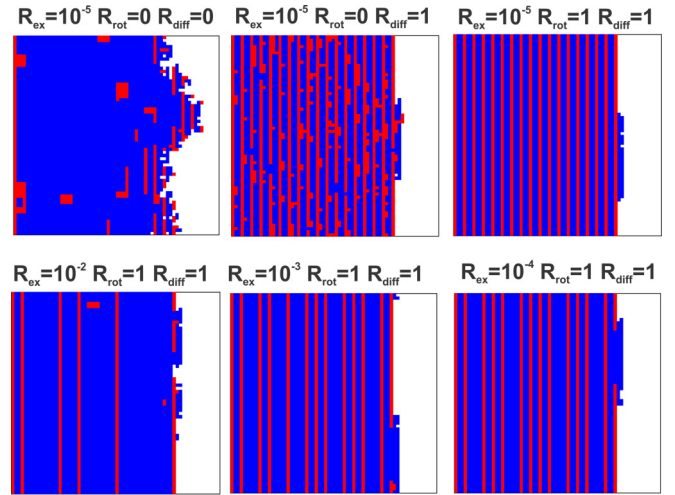


FIG. 6. Effect of rates of exchange (R_{ex}), diffusion (R_{diff}), and rotation (R_{rot}) on growth mode. Top: rotation is necessary to obtain near-perfect order. Bottom: Decreasing the exchange rate increases order. Energy parameters used for all the simulations (in eV): $\mu = 3$, $\epsilon_s = 3$, $\epsilon_d = 1$, $\Delta_r = 2$, $\Delta_b = 1$, $\tilde{\Delta}_r = 1$, and $\tilde{\Delta}_b = 2$.

phase of ZnTPP on Ag(100). Upon annealing, this structure transforms into the thermodynamically stable homogeneous phase. We have used a statistical mechanical model to propose a simple physical explanation for this behavior. If molecule-substrate forces favor inhomogeneity but molecule-molecule forces favor homogeneity, then the former can “win” at the growth front, where molecules have one or two intermolecular contacts, while the latter can win in the interior of the grown structure, where molecules have four intermolecular contacts. This simple mechanism is likely to be relevant to other examples of growth on a structured surface and might be exploited to grow specific kinetically controlled patterns.

ACKNOWLEDGMENTS

S.R., P.K., C.R., and R.A.B. acknowledge funding from the National Science Foundation under Award No. CHE-1446389. S.W. performed work at the Molecular Foundry, supported by the Office of Science, Office of Basic Energy Sciences, of the U.S. Department of Energy under Contract No. DE-AC02-05CH11231.

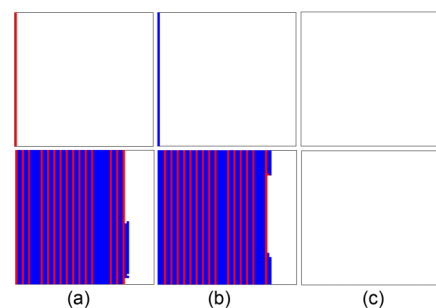


FIG. 7. Growth simulated for different seed columns for $k_B T = 26$ meV: (a) red column, (b) blue column, and (c) empty column. Parameter set (in eV): $\mu = 3$, $\epsilon_s = 3$, $\epsilon_d = 1$, $\Delta_r = 2$, $\Delta_b = 1$, $\tilde{\Delta}_r = 1$, and $\tilde{\Delta}_b = 2$. Rates: $R_{\text{ex}} = 10^{-5}$, $R_{\text{diff}} = 1$, and $R_{\text{rot}} = 1$.

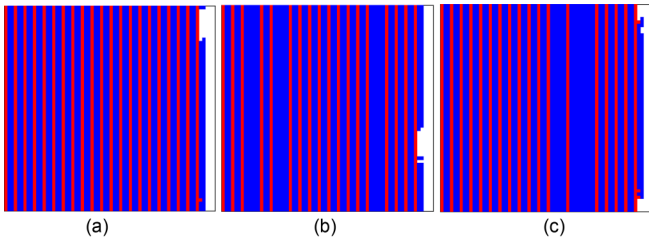


FIG. 8. Stacking faults similar to those seen in experiment. (a)–(c) Distinct growth processes for the same set of parameters (in eV): $\mu = 3$, $\epsilon_s = 3$, $\epsilon_d = 1$, $\Delta_r = 2$, $\Delta_b = 1$, $\tilde{\Delta}_r = 1$, and $\tilde{\Delta}_b = 2$. Rates: $R_{\text{ex}} = 10^{-5}$, $R_{\text{diff}} = 1$, and $R_{\text{rot}} = 1$.

APPENDIX: MONTE CARLO GROWTH PROCEDURE

1. Algorithm

The growth algorithm, adapted from Ref. [32], is as follows. Select at random a lattice site. If the site is vacant, propose to occupy it with a particle (red or blue, with equal likelihood). If the site is instead occupied, propose a diffusion move with probability P_{diff} , a rotation move with probability P_{rot} , or a removal with probability P_{ex} . A diffusion move consists of proposing to move the particle to a randomly chosen nearest-neighbor site. A rotation move consists of proposing a change of color (orientation) of the particle. A removal move consists of proposing to make the site vacant. We relate these probabilities to rates R via

$$P_{\text{ex}} = R_{\text{ex}}/\Sigma, \quad P_{\text{diff}} = R_{\text{diff}}/\Sigma, \quad P_{\text{rot}} = R_{\text{rot}}/\Sigma, \quad (\text{A1})$$

where $\Sigma \equiv R_{\text{ex}} + R_{\text{diff}} + R_{\text{rot}}$. For most calculations in the paper we set $R_{\text{ex}} = 10^{-5}$ and $R_{\text{rot}} = R_{\text{diff}} = 1$. Molecular rotation and diffusion at the surface therefore occur several orders of magnitude faster than molecular adsorption, as expected for our experimental conditions. Figure 6 shows the effect of

changing these rates on the growth mode for a given set of interaction energies.

To enforce a detailed balance with respect to the energy function described in the text, we accepted these moves with probabilities

$$\begin{aligned} P_{\text{occupy}}^{\text{acc}} &= \min(1, 2P_{\text{ex}}e^{-\beta\Delta E}), \\ P_{\text{remove}}^{\text{acc}} &= \min\left(1, \frac{1}{2P_{\text{ex}}}e^{-\beta\Delta E}\right), \\ P_{\text{diff}}^{\text{acc}} &= \min(1, e^{-\beta\Delta E}), \\ P_{\text{rot}}^{\text{acc}} &= \min(1, e^{-\beta\Delta E}), \end{aligned} \quad (\text{A2})$$

where ΔE is the energy change upon proposing the move. At room temperature, $\beta = 1/(k_B T) = 1/26 \text{ meV}^{-1}$.

To promote annealing (postgrowth) to the thermodynamically stable state we added a move in which a site was chosen at random and made red, blue, or vacant with equal probabilities. This move was accepted with the usual Metropolis probability $\min(1, e^{-\beta\Delta E})$.

2. Choice of initial conditions

We explored the role of initial conditions by starting from an empty surface or a single red or blue column (frozen during empty simulations). Seeding can be related to the initial attachment of molecules at the step edges and is summarized in Fig. 7. Under the conditions explored below, seeding with red or blue molecules does not prevent or significantly alter the growth of a striped $[2 + 1]$ phase. For the conditions studied, the absence of seeds prevents growth initiation because the nucleation barrier for line initiation is too large to overcome in the time of the simulation.

3. The $[2 + 1]$ phase stacking fault during growth

During the growth of a $[2 + 1]$ phase we observed occasional stacking errors, typically characterized by entire miss-

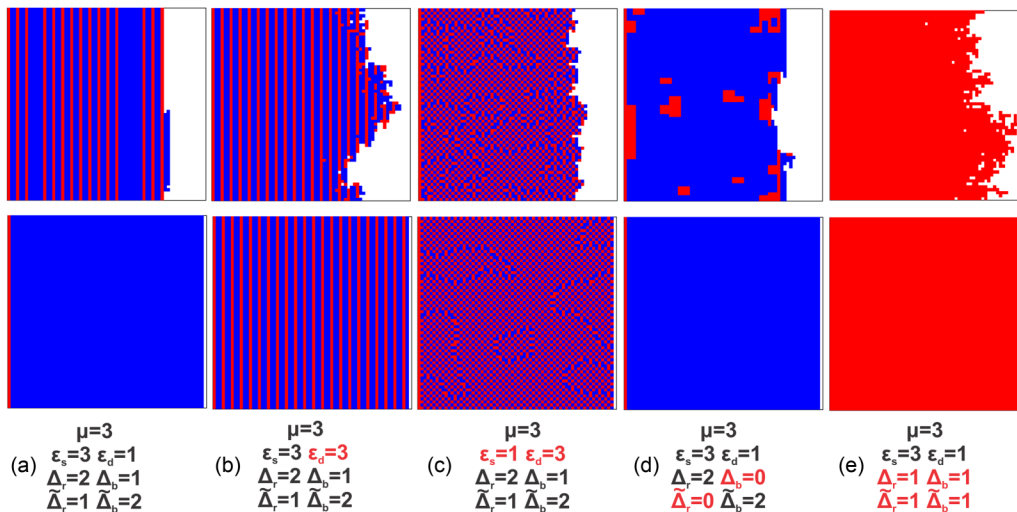


FIG. 9. Simulated grown structures immediately upon reaching 80% coverage (top) and after annealing to equilibrium (bottom) for different parameter sets. Highlighted in red are the parameters that have been changed with respect to case (a). Rates: $R_{\text{ex}} = 10^{-5}$, $R_{\text{diff}} = 1$, and $R_{\text{rot}} = 1$.

ing red rows (see Fig. 8). Such features are similar to those seen in experiment, indicating the importance of a templating effect at the growth front.

4. Accessible phases

Alternative outcomes of the simulations can be generated for different energy parameters, as seen in Figs. 9(b) to 9(e), indicating that, as expected from our simple analytic arguments, only a limited phase space allows for the stabi-

lization of a kinetically trapped $[2 + 1]$ phase transforming to a thermodynamically favored square phase. In Fig. 9(b), the molecular interaction energies ϵ_s and ϵ_d are set equal, and the resulting order is dominated by the substrate-induced molecular stripes. Although fewer defects are generated during growth of the $[2 + 1]$ phase, the thermodynamically favored phase is also $[2 + 1]$. In Figs. 9(c) to 9(e), tuning either intermolecular interactions or molecule-substrate interactions can lead to a checkerboard arrangement, to phase segregation between red and blue islands, or to pure red phases.

-
- [1] C. Wackerlin, K. Tarafder, D. Siewert, J. Girovsky, T. Hahlen, C. Iacovita, A. Kleibert, F. Nolting, T. A. Jung, P. M. Oppeneer, and N. Ballav, *Chemical Science* **3**, 3154 (2012).
- [2] F. Yang, C. Li, Y. Wei, N. Yan, X. Wang, F. Liu, S. You, J. Wang, W. Ma, and W. Li, *Macromol. Rapid Commun.* **39**, 1800546 (2018).
- [3] C. Chen, T. Joshi, H. Li, A. D. Chavez, Z. Pedramrazi, P.-N. Liu, H. Li, W. R. Dichtel, J.-L. Bredas, and M. F. Crommie, *ACS Nano* **12**, 385 (2018).
- [4] D. Arnold, D. Manno, G. Micocci, A. Serra, A. Tepore, and L. Valli, *Thin Solid Films* **327–329**, 341 (1998).
- [5] A. Tepore, A. Serra, D. Manno, L. Valli, G. Micocci, and D. P. Arnold, *J. Appl. Phys.* **84**, 1416 (1998).
- [6] J. Kim, S.-H. Lim, Y. Yoon, T. D. Thangadurai, and S. Yoon, *Tetrahedron Lett.* **52**, 2645 (2011).
- [7] L. Wang, H. Li, J. Deng, and D. Cao, *Current Organic Chemistry* **17**, 3078 (2013).
- [8] R. McGuire Jr., D. K. Dogutan, T. S. Teets, J. Suntivich, Y. Shao-Horn, and D. G. Nocera, *Chem. Sci.* **1**, 411 (2010).
- [9] D. K. Dogutan, R. McGuire, and D. G. Nocera, *J. Am. Chem. Soc.* **133**, 9178 (2011).
- [10] F. Calle-Vallejo, J. Martnez, J. Garca-Lastra, E. Abad, and M. Koper, *Surf. Sci.* **607**, 47 (2013).
- [11] M. R. Wasielewski, *Chem. Rev.* **92**, 435 (1992).
- [12] W. M. Campbell, A. K. Burrell, D. L. Officer, and K. W. Jolley, *Coordination Chemistry Reviews* **248**, 1363 (2004).
- [13] A. Yella, H.-W. Lee, H. N. Tsao, C. Yi, A. K. Chandiran, M. Nazeeruddin, E. W.-G. Diau, C.-Y. Yeh, S. M. Zakeeruddin, and M. Gratzel, *Science* **334**, 629 (2011).
- [14] M. Urbani, M. Gratzel, M. K. Nazeeruddin, and T. Torres, *Chem. Rev.* **114**, 12330 (2014).
- [15] J. V. Barth, G. Costantini, and K. Kern, *Nature (London)* **437**, 671 (2005).
- [16] J. A. Elemans, S. Lei, and S. De Feyter, *Angew. Chem., Int. Ed.* **48**, 7298 (2009).
- [17] G. Franc and A. Gourdon, *Phys. Chem. Chem. Phys.* **13**, 14283 (2011).
- [18] M. Lackinger and W. Heckl, *J. Phys. D* **44**, 464011 (2011).
- [19] W. Auwarter, D. cija, F. Klappenberger, and J. V. Barth, *Nat. Chem.* **7**, 105 (2015).
- [20] Q. Fan, J. M. Gottfried, and J. Zhu, *Acc. Chem. Res.* **48**, 2484 (2015).
- [21] L. Scudiero, D. E. Barlow, and K. W. Hipps, *J. Phys. Chem. B* **104**, 11899 (2000).
- [22] J. M. Gottfried, *Surf. Sci. Rep.* **70**, 259 (2015).
- [23] C. Ruggieri, S. Rangan, R. A. Bartynski, and E. Galoppini, *J. Phys. Chem. C* **119**, 6101 (2015).
- [24] C. Ruggieri, S. Rangan, R. A. Bartynski, and E. Galoppini, *J. Phys. Chem. C* **120**, 7575 (2016).
- [25] D. Wechsler, M. Franke, Q. Tariq, L. Zhang, T.-L. Lee, P. K. Thakur, N. Tsud, S. Bercha, K. C. Prince, H.-P. Steinruck, and O. Lytken, *J. Phys. Chem. C* **121**, 5667 (2017).
- [26] I. Horcas, R. Fernandez, J. M. Gomez-Rodriguez, J. Colchero, J. Gomez-Herrero, and A. M. Baro, *Rev. Sci. Instrum.* **78**, 013705 (2007).
- [27] S. Mullerger, M. Rashidi, T. Lengauer, E. Rauls, W. G. Schmidt, G. Knor, W. Schofberger, and R. Koch, *Phys. Rev. B* **83**, 165416 (2011).
- [28] W. Auwarter, K. Siefert, F. Bischoff, D. cija, S. Vijayaraghavan, S. Joshi, F. Klappenberger, N. Samudrala, and J. V. Barth, *Nat. Nanotechnol.* **7**, 41 (2012).
- [29] G. Rojas, S. Simpson, X. Chen, D. A. Kunkel, J. Nitz, J. Xiao, P. A. Dowben, E. Zurek, and A. Enders, *Phys. Chem. Chem. Phys.* **14**, 4971 (2012).
- [30] F. Buchner, K. Seufert, W. Auwarter, D. Heim, J. V. Barth, K. Flechtner, J. M. Gottfried, H.-P. Steinruck, and H. Marbach, *ACS Nano* **3**, 1789 (2009).
- [31] M. O. Sinnokrot, E. F. Valeev, and C. D. Sherrill, *J. Am. Chem. Soc.* **124**, 10887 (2002).
- [32] S. Whitlam, L. O. Hedges, and J. D. Schmit, *Phys. Rev. Lett.* **112**, 155504 (2014).
- [33] P. Donovan, A. Robin, M. S. Dyer, M. Persson, and R. Raval, *Chem. Eur. J.* **16**, 11641 (2010).
- [34] H. Tang, N. Tarrat, V. Langlais, and Y. Wang, *Beilstein J. Nanotechnol.* **8**, 2484 (2017).